Top Med Chem (2020) 34: 33–54
DOI: 10.1007/7355_2019_88

Published online: 29 February 2020

Organic Fluorescent Probes for Diagnostics and Bio-Imaging

Xingyue Yang, Jonathan F. Lovell, Niren Murthy, and Yumiao Zhang

Contents

X. Yang
School of Chemical Engineering and Technology, Tianjin University, Tianjin, China

J. F. Lovell
Department of Biomedical Engineering, State University of New York at Buffalo, Buffalo, NY, USA

N. Murthy
Department of Bioengineering, University of California, Berkeley, CA, USA

Y. Zhang (✉)
School of Chemical Engineering and Technology, Tianjin University, Tianjin, China

Department of Bioengineering, University of California, Berkeley, CA, USA
e-mail: ymzhang88@tju.edu.cn

Abstract Fluorescence bio-imaging holds potential for new approaches for disease detection and diagnosis. Compared with conventional clinical contrast imaging modalities, such as X-ray and MRI, which use contrast agents that are "always on," fluorescence imaging contrast agents can readily be designed to be activatable under specific circumstances and also can be used in multiplexed imaging schemes. While a wide variety of fluorescence imaging probes have been developed, small organic fluorescence probes have the advantages of being robustly synthesized and characterized, as well as a track record for clinical translation. In this chapter, we discuss organic fluorophores and highlighted some examples of their biological applications. The aim of this chapter is to provide a literature review of the development of organic fluorescent probes for biomedical imaging and diagnosis.

Keywords Disease diagnosis, Fluorescence imaging, Fluorescence probes, Imaging modalities, Organic fluorophores

1 Introduction

Near-infrared fluorescence imaging has developed as a powerful optical imaging modality for visualization of molecular process and biological activities, which uses a low-light camera to collect fluorescence emission from fluorophores [1]. The fluorescence imaging technique is based on the fact that the transillumination of light through normal tissue is significantly different from that through an object (e.g., tumor or infected tissues). Compared to other well-developed imaging techniques such as X-ray, computed tomography (CT) [2], magnetic resonance imaging (MRI), and ultrasound [3], fluorescence imaging is advantageous because of high sensitivity, excellent resolution, and minimum photodamage to tissues [4]. Fluorescence imaging has been widely applied for real-time detection of biological species [5–8]. One challenge of imaging biology in its native physiological state using fluorescence imaging method is the autofluorescence. Scattered light generated a noise background that might even wash out the image of targets [9]. In addition, most of the traditional fluorescent probes have absorption and emission in UV-Vis range; however, interference from absorption by hemoglobin, myoglobin, and other heme proteins is significantly high, leading to light scattering and impaired tissue penetration [10]. Therefore, NIR (700–1,000 nm) light was recommended for wavelength selection for body imaging [11]. Meanwhile, in recent years, dyes in the second near-infrared region (NIR-II, 1,000–1,700 nm) have been explored with a number of merits over the NIR-I imaging modalities in terms of reduced photon scattering and improved penetration depth [12–14], as well as good sensitivity, enhanced spatial resolution, and better safety profile [15, 16]. A wide variety of NIR excitable fluorescence contrast agents have been developed for targeting and diagnosis of cancers, inflammation, and other tissue abnormalities. Representative contrast agents

of fluorescence imaging include inorganic nanoparticles, quantum dots, fluorescent protein, and organic fluorophores. While inorganic materials account for an important category of fluorescent contrast materials, the main focus of this chapter is limited to organic fluorophore developments, followed by some examples of common biological applications.

2 Representative Organic Fluorophores

Organic fluorophores are widely used as contrast agents in optical microscopy. Numerous fluorophores have been developed for fluorescence imaging. In this section, we will summarize some commonly used organic fluorophores including cyanines, 5-aminolevulinic acid (5-ALA), methylene blue (MB), difluoroboron dipyrromethene (BODIPY), rhodamine, nicotinamide adenine dinucleotide (NADH), flavin adenine dinucleotide (FAD), porphyrins, phthalocyanines (Pcs), naphthalocyanines (Ncs), etc. Their backbone chemical structures were illustrated in Fig. 1.

2.1 Cyanines

Cyanine dyes represent a large family of fluorescent compounds with the chemical structure of two aromatic or heterocyclic rings connected with a polymethine chain. Cyanines and their derivatives are a common source of organic fluorophores with excitation wavelength in the range of 600–900 nm [17]. Among them, indocyanine green (ICG) is a widely used fluorophore that has been approved by FDA for medical use. Compared to other dyes such as Cy5, ICG has longer emission wavelength so that it has deeper penetration and less autofluorescence. ICG was initially used for medical imaging because of its minimal toxicity [18]. It has also been used for cardiovascular function test, retinal angiography, and hepatic clearance, as well as for sentinel lymph node mapping, coronary arteriography during cardiac bypass surgery [19], cholangiography during hepatobiliary surgery [20–22], and blood flow measurement during aneurysm surgery [23]. Based on the characteristics of ICG, one FDA-approved intraoperative fluorescent imaging system (Novadaq Technologies, SPY system) has been developed. The whole system comprises an 806 nm laser to excite ICG and camera unit, monitor, central processing unit, and laser generator. For image acquisition, the camera was positioned about 30 cm above the place of interest. An automatic distance sensor can indicate the correct position to ensure the camera is at the right place. After injection of ICG, the laser is activated, and image acquisition is started by a single command to the computer. For example, in one study, Novadaq SPY system was used for quality assessment in off-pump coronary artery bypass grafting [21]. This is based on the fact that ICG can bind to plasma proteins and protein-ICG complex emits light

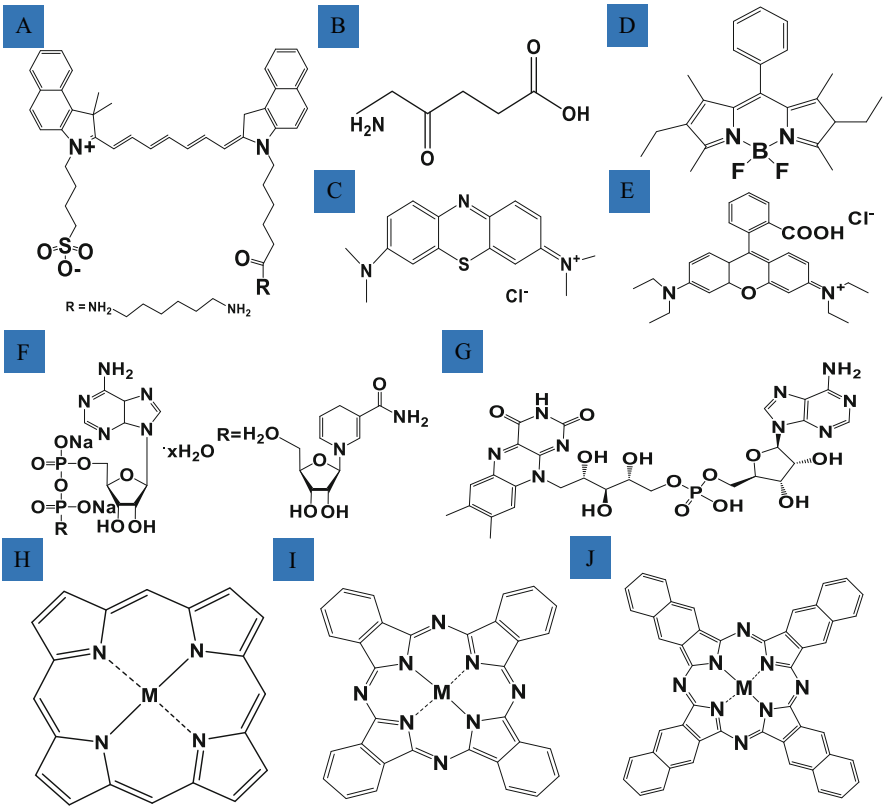

Fig. 1 Chemical structures of (**a**) indocyanine green (ICG); (**b**) 5-aminolevulinic acid (5-ALA); (**c**) methylene blue (MB); (**d**) difluoroboron dipyrromethene (BODIPY); (**e**) rhodamine B; (**f**) nicotinamide adenine dinucleotide (NADH); (**g**) flavin adenine dinucleotide (FAD); (**h**) porphyrins; (**i**) phthalocyanines (Pcs); (**j**) naphthalocyanines (Ncs) (M = 2H or metal)

at the wavelength of around 830 nm. Thirty-eight patients undergoing surgery were included and 107 grafts were analyzed. ICG-based SPY system was shown to be easy to handle with minimal adverse effects.

2.2 5-Aminolevulinic Acid (5-ALA)

5-ALA is a precursor for the heme biosynthesis. After taking up cells, 5-ALA produces a photoactive protoporphyrin IX (PpIX), which is preferentially accumulated in cancer cells [24–26]. 5-Aminolevulinic acid (5-ALA) has been used for intraoperative mapping and monitoring the efficiency of complete resection of enhancing tumor (CRET) and gross total resection (GTR). Schucht et al. have used 5-ALA-induced fluorescence as guidance during tumor resection. 20 mg/kg

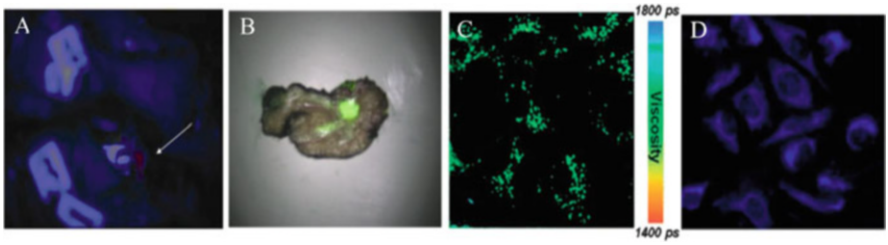

Fig. 2 Fluorescence imaging using various organic probes. (**a**) Fluorescence imaging guided by 5-ALA (white arrow indicated corticospinal tract in a right motor area) (Adapted from the Ref. [28] with permission); (**b**) a clear fluorescent spot was seen at the site of tumor with methylene blue as contrast agent (Adapted from the Ref. [29] with permission); (**c**) fluorescence lifetime image of SK-OV-3 cells with BODIPY as contrast agent (Adapted from the Ref. [35] with permission); (**d**) fluorescence images of RAW cells co-stained fluorescent imidazo[1,5-a]pyridine-rhodamine probe (Adapted from the Ref. [40] with permission)

5-ALA was administered 3 h prior to anesthesia, and resection was conducted until all fluorescence was completely removed while preserving neurological function. Consequently, high rate of CRET and GTR was achieved [27]. However, increasing resection toward the abnormality border might lead to neurological defects such as brain tissue injury or vascular injury. In addition, 5-ALA was used for imaging-guided surgery of high-grade gliomas in eloquent areas. For example, in one study, assisted by 5-ALA fluorescence and monitoring, gross total resection (GTR) $> 98\%$ and GTR $> 90\%$ were observed in 93% and 100% of cases, respectively [28] (see Fig. 2a).

2.3 Methylene Blue

Methylene blue (MB), also known as methylthioninium chloride, is commonly used as medication for the treatment of methemoglobinemia or as dyes for contrast imaging. MB is used for several clinical indications. Also, as a NIR fluorescent dye, methylene blue could be used to detect breast cancer intraoperatively. Twenty-four patients with breast cancer were investigated. The mini-FLARE imaging system was employed to provide NIR fluorescence during surgery. It was found that 20 out of 24 (83%) patients of breast tumors were detected in resected specimen by MB fluorescence imaging method and the concordance of fluorescence signal and tumor tissue was confirmed by histology [29] (see Fig. 2b). Another example is using MB for intraoperative NIR fluorescence imaging of parathyroid adenomas. 0.5 mg/kg MB was administered into 12 patients undergoing parathyroid surgery. Mini-FLARE imaging system was used. Ten out of twelve patients are identified to have parathyroid adenoma, and nine out of these patients, parathyroid adenoma could be clearly detected by NIR fluorescence using MB [30]. And this was the first study showing that low-dose MB can be used to identify parathyroid adenomas.

2.4 BODIPY

BODIPY (4,4-difluoro-4-bora-3a,4a-diaza-s-indacene, or difluoroboron dipyrromethene) has gained notoriety for its excellent photostability and chemical stability and high molar absorption coefficient and fluorescence quantum yield [31]. A wide variety of BODIPY-based fluorescent dyes have been developed, and some of them are commercially available such as ER-Tracker Green and LysoTracker Red. The photophysical properties of BODIPY are tuned by conjugation of various chemical residues on the difluoroboron dipyrromethene backbone. For example, (a) 2,6-positions are available for the electrophilic substitution reactions for the introduction of bromine or iodine [32] for further synthetic modification; (b) active methyl groups at 3,5-position are subject to chemical modification owing to their strong nucleophilic character [33]; (c) nucleophilic substitution of leaving groups is also great modification site for a thiomethyl group, for example, at the 8-position [34]; (d) a halogen atom could be used for further extension of the conjugation or the structure via palladium-catalyzed coupling reaction; (e) extension of Pi electron conjugation; and (f) modification at the boron center. Readers are referred to these comprehensive review papers that have described the synthesis and photophysical properties of BODIPY [35–37] (see Fig. 2c). BODIPY could be used for many biological applications such as indicators of pH, ion, biomolecules (e.g., peptide, thiol, saxitoxin), reactive oxygen species and reactive nitrogen species, and others (e.g., hydrolysis esters, biocatalytic reactions).

2.5 Rhodamine

Rhodamine is another fluorescent dye used for bio-imaging, and many rhodamine-based imaging systems have been developed. For example, a sugar-rhodamine fluorescent probe was designed as a specific sensor for Cu^{2+}, exhibiting fluorescent color changes by naked eye. More importantly, the probe also could detect the Cu^{2+} at 0.2 mg/L concentration, which is ten times lower than minimum Cu^{2+} value (2.0 mg/L) in drinking water recommended by WHO [38]. Another chemosensor system based on the conjugation of rhodamine with quinoline was developed for the detection of Cu^{2+} and Fe^{3+} in vivo with good selectivity and sensitivity [39]. In addition, a ratiometric fluorescent probe (RIM) based on fluorescence resonance energy transfer (FRET) was synthesized from imidazo[1,5-a] pyridine and rhodamine for the detection of HOCl. Without HOCl, the RIM displayed absorption spectra at 360 nm, whereas, in the presence of HOCl, ring-opening form of rhodamine moiety resulted in the FRET process with imidazo[1,5-a] pyridine as donor and rhodamine as acceptor, showing an additional absorption peak at 560 nm. The detection range is 0–5 μM with high selectivity and sensitivity [40] (see Fig. 2d). Another novel rhodamine derivative fluorescent probe (RDP) was synthesized through the reaction of rhodamine B derivative with di(pyridin-2-yl)methanone in

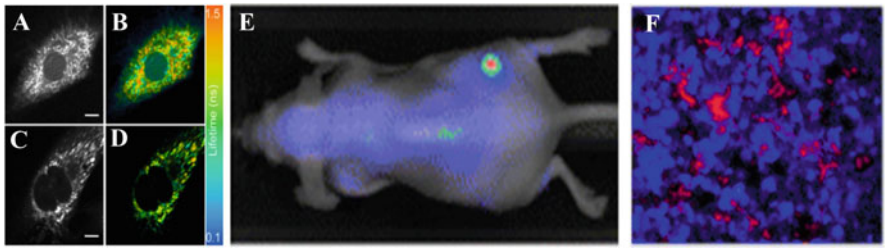

Fig. 3 Fluorescence imaging using various organic probes. Two-photon autofluorescence lifetime imaging reveals heterogeneous environment of the intracellular NADH in breast cancer (**a**, **b**) and normal cells (**c**, **d**) (Adapted from the Ref. [45] with permission); silicon naphthalocyanine (SiNc) polymeric nanoparticles could be used for imaging (**e**) and phototherapy (**f**) with good fluorescence contrast (Adapted from the Ref. [67] with permission)

ethyl alcohol. This study found that RDP exhibited nonfluorescent properties itself; however, a new fluorescence spectrum peak of RDP at 560 nm was observed in the presence of trivalent metal ions (M^{3+}) (where $M^{3+} = Fe^{3+}$, Al^{3+}, and Cr^{3+}), with the color change from colorless to pink, resulting from the ring-opened RDP-M^{3+} complex [41].

2.6 NADH and FAD as Endogenous Fluorophores

Various endogenous chromophores existing in cells and tissues play important role in metabolic activities and cell functions. Common endogenous fluorophores include retinol, tryptophan, elastin, collagen, and porphyrins [42]. Among them, nicotinamide adenine dinucleotide (NADH) and flavin adenine dinucleotide (FAD) are most extensively investigated. For example, using the intracellular NADH as contrast agent, breast cancer cells are easily differentiated from normal cells under two-photon autofluorescence lifetime imaging system [43–46] (see Fig. 3a–d). The redox states of endogenous fluorophores NADH and FAD can be measured as a direct indicator of oxygen amount in the cells. The reduced form (NADH) acts ubiquitously as electron carrier that plays significant role in both oxidative metabolism and glycolysis, and it is naturally fluorescent, whereas the oxidized form (NAD^+) is fluorescently quenched [47]. Another pair of redox markers is FAD/FADH that exhibits the opposite effect. Yaseen et al. used two-photon fluorescence lifetime microcopy of NADH for imaging of cerebral energy metabolism [48]. They found that using NADH as fluorescence probe, four different components responded to anoxia and indicated different enzymatic formulations [48]. In addition, to monitor the conformational and functional states of NADH, fluorescence lifetime imaging microscopy (FLIM) has been developed that is based on the measurement of the time fluorescent molecules stayed in their excited states. One important feature of FLIM is that the lifetime of a chromophore keeps

unchanged, which is advantageous for quantification of ion concentrations and biological environment [49–55].

2.7 Porphyrins, Phthalocyanines (Pcs), and Naphthalocyanines (Ncs) and Their Nanosystems

Most porphyrins, Pcs, and Ncs are hydrophobic. To improve their solubility, polymeric nanoparticles, liposomes, and chemical modification are employed. Liposomes have proven biocompatibility, whereas polymeric nanoparticles are readily available for a range of chemical modifications. Porphyrins can emit fluorescence in the NIR range that can be used for in vivo imaging. The first use of porphyrin fluorescence for tumor detection can date back to as early as 1924 [56]. Auler and Banzer found that hematoporphyrins can be preferentially accumulated in tumors and lymph nodes. Following studies also found that porphyrins show great affinity for neoplastic tissue [57]. Porphyrin fluorescence imaging could be used to assess the success or failure of photodynamic therapy [58, 59] or imaging-guided surgical tumor resection [60]. Another important fluorescence imaging example is that compared with hematoporphyrins, tetratraphenylporphinesulfonate (TPPS) that was found to better localize in tumor [61]. Porphyrin and phospholipid conjugates were also synthesized that can form self-assembled organic nanoparticles (termed porphysome) [62]. Porphysomes exhibit liposome-like structure with high loading capacity, high absorption of NIR light, and excellent biocompatibility. Owing to the presence of porphyrin, porphysomes enabled the visualization of lymph nodes by photoacoustic imaging, and also the fluorescence could be restored upon dissociations, enabling low-background fluorescence imaging. In addition, various porphyrin-PEG conjugates were also made for fluorescence imaging application [63, 64]. Compared to porphyrins, Pcs and Ncs typically show higher extinction coefficient and longer absorption wavelengths because of additional aromatic rings fused to pyrrolic subunits. In addition, Pcs also show promise in photodynamic therapy for cancers [65]. Zinc phthalocyanine (ZnPc) was encapsulated in liposomes by solvent exchange method for fluorescence imaging of tumor. After introducing into blood intravenously, ZnPc liposomes was taken up by lipoprotein and then accumulated in the tumor; after 120 min, the fluorescence in the tumor and blood reached a plateau [66]. Recently, silicon naphthalocyanine (SiNc) polymeric nanoparticles have been synthesized for fluorescence imaging and photodynamic therapy [67] (see Fig. 3e, f). SiNc was loaded in poly(ethylene glycol)-poly (ε-caprolactone) (PEG-PCL) copolymers. It was demonstrated that Nc polymeric nanoparticles have good photostability. Silicon 2,3-naphthalocyanine bis (trihexylsilyloxide) (NIR775) was co-loaded with 2,3-bis(4-(phenyl(4-(1,2,2-triphenylvinyl)phenylamino)phenyl)fumaronitrile (TPETPAFN) into DSPE-PEG2000. Taking advantage of FRET between NIR775 and TPETPAFN, the fluorescence of the nanoparticles was enhanced by 47-fold compared to excitation

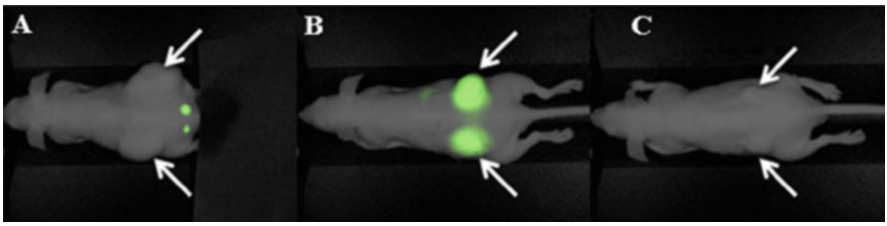

Fig. 4 Fluorescence imaging of antibody-IRDye conjugates. Mice were imaged at different time points to determine optimal imaging time after administration of Claudin-1-IRDye800CW (**a**) 24 h, (**b**) 48 h, and (**c**) 72 h. Arrows point to tumors on the bilateral flanks (Adapted from the Ref. [71] with permission)

of NIR775 alone. This nanoplatform also showed photostability and low cytotoxicity.

2.8 Antibody Conjugates

Antibody-IR dye conjugates or antibody conjugated nanoparticles are playing an important role in the medicine field [68, 69]. Monoclonal antibodies have been conjugated to a wide variety of nanoplatforms such as micelles, liposomes, nanoparticles, and many others [70]. Among them, indocyanine green (ICG) was widely used for molecular imaging via effective perfusion into tissues, which provides a great pathway for fluorescence imaging-guided surgical operations. And antibody IR dye probes could specifically target the diseased tissue clearly. Claudins, which are important proteins acting as epithelial barrier in colon cells, are overexpressed for the development of colon cancer; therefore, conjugation of claudin antibody with IR800CW had great potential in clinical practice. As shown in Fig. 4, in one colon tumor study, tumor margin in mice administered with Claudin-1-IRDye800CW could be clearly visualized after 48 h and 72 h without significant background signal. More importantly, visualization of local metastases could be achieved with anti-claudin antibody conjugating with IR800CW as contrast agent, and no noticeable side effects or toxicity on organs were observed [71]. CEA (carcinoembryonic antigen) is another representative target example, and its overexpression was found in 90% colorectal cancer cells and could be the specific target for colorectal cancer diagnosis and treatment in intraoperation. Photosensitizer phthalocyanine dye IR700 was found to be cytotoxic once exposed to NIR light irradiation, and a study on treatment of pancreatic cancer revealed that the conjugation of phthalocyanine dye IR700 with anti-CEA antibody could effectively target pancreatic tumor cells and kill most of the tumor cells upon NIR light activation [72, 73]. Fluorescent dye-antibody conjugates also show great promise in clinical performance. For example, SGM-101, the CEA antibody, has been used in clinical detection of colorectal cancer without significant adverse events related to antibody

fluorescent probes; and in a study based on 26 patients, 98% sensitivity and 84% accuracy in the expansion cohort were achieved [74]. Other antibody-NIR dye conjugates such as IRDye 800CW or Alexa Fluor 680 also show good clinical performance [75]. Therefore, NIR antibody combination is a powerful tool in diagnosis of tumor cells and metastases with high specificity and availability, providing useful information for decision-making during clinical surgery.

3 Biological Applications

3.1 Imaging-Guided Surgery

Fluorescence molecular imaging has been developed as an emerging tool for imaging-guided surgery. For precise intraoperative positioning, a fluorescent fluorophore coupled with an imaging system will be used to help surgeons to differentiate normal tissues and malignant tissues. Imaging-guided surgeries have been used for better treatment for liver metastases [76], cervical cancer [77, 78], melanoma [79, 80], ovarian cancer [81], and vulvar cancer [77]. After injection of fluorescent contrast agents, imaging guiding system indirectly activates fluorescent contrast agents with NIR light, followed by image registration processing, providing video-rate images. The imaging contrast agents and surgical navigation systems are two most important components of fluorescence molecular imaging technology. With respect to contrast agents, indocyanine green is a commonly used FDA-approved dye. It has been used in sentinel lymph node mapping [82] and hepatic micrometastases detection [83]. In addition, 5-aminolevulinic acid (5-ALA) was also orally administered to better detect patients with glioma [84]; Alexa-647 was also used to assess tumor margins and better detect head and neck squamous cell carcinoma [85]. Also, in order to selectively detect tumor, fluorescent contrast agents were also conjugated with targeting moieties such as sugars, peptides, or antibodies [86]. As of surgical navigation systems, there are several surgical navigation systems existing for clinical studies including SPY, Artemis, Photodynamic Eye, Fluobeam, SurgOptix, FLARE, and GXMI Navigator. SPY system has been utilized to monitor skin perfusion using ICG as contrast agent during nipple-sparing mastectomies [87]. FLARE™ imaging systems were created that use three cameras and collect signals from two NIR channels. FLARE™ imaging systems are mostly used for intraoperative SLN mapping and cancer surgeries [88, 89]; Artemis™ can collect both color images and the fluorescent overlay, providing a powerful tool for nerve surgery. For more detailed surgical navigation systems, readers are referred to these comprehensive review papers [90, 91]. For example, compared with the white-light reflectance imaging, the image of main nerve trunk and small branches in muscle planes was better visualized under fluorescent imaging with organic probes injected (see Fig. 5).

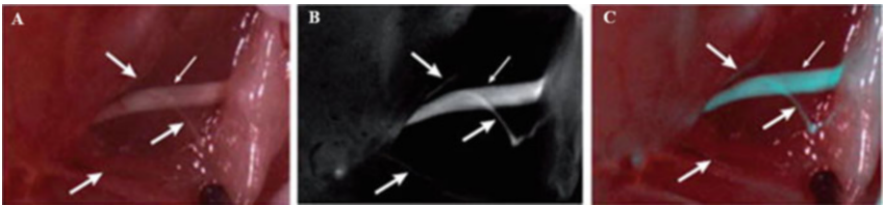

Fig. 5 White-light reflectance image and the fluorescence image of sciatic nerve branching within muscle planes. (**a**) A white-light reflectance image of a sciatic nerve branching within muscle planes. The main trunk of the nerve was clearly imaged (thin white arrow), but the smaller branches were difficult to distinguish from surrounding tissue (thick white arrows); (**b**) a fluorescence image clearly showing both the main nerve trunk and small branches using fluorescent contrast agent; (**c**) an overlay of fluorescence and white-light reflectance images (Adapted from the Ref. [87] with permission)

3.2 Thiol Detection

Bio-thiols such as cysteine (Cys), homocysteine (Hcy), and glutathione (GSH) as necessary reactive sulfur species play an indispensable role in cellular activity [92–94]. For example, GSH can regulate the cellular redox activities, signal transduction, and gene expression [95], whereas Cys and Hcy are the precursors of hydrogen sulfide. Many diseases including cancers can be possibly caused by the abnormally high levels of intracellular Cys [96]. Elevated amount of homocysteine might give rise to Alzheimer's disease or inflammatory bowel diseases. Therefore, accurate detection of intracellular thiols is intriguing for disease diagnosis. A fluorescein-based fluorescent probe was synthesized by conjugation of 2-cyclopentenone to fluorescein-monoaldehyde in the presence of imidazole in THF for the detection of various thiol-containing analytes including Cys, Hcy, GSH, Gly, Phe, Ser, Glu, Lys, Arg, His, Ala, Gln, Met, Tyr, and cysteine. This probe itself is nonfluorescent, but after addition of Cys, Hcy, and GSH, stronger fluorescence intensity and greater UV-Vis spectral changes occurred because of the formation of thioether. The probe itself is nonfluorescent without GSH, but after addition of GSH under neutral and basic conditions, a new emission peak was observed, and the fluorescence intensity was increased by 61-fold. This probe was also applied to monitor thiols in cells and independent tissues and organs of zebra fish. Strong fluorescence was observed from murine P19 embryonic carcinoma cells and 3-day-old zebra fish after incubation with 20 μM of the probe [97] (see Fig. 6a). Another example is 4-aminonaphthalimide dimer connected by a disulfide linker that can detect thiol quantitatively. Once thiol triggers the cleavage of the disulfide group, 4-aminonaphthalimide is released, and its fluorescence can be restored showing jade green color seen by naked eyes. This probe was also applied successfully for the thiol imaging in living HeLa cells without pH interference [98]. Also, two-photon fluorescent probe could be used to detect the thiols in mitochondria in live cells and living tissues at 90–190 μm depth. Compared to one-photon microscopy, two-photon microscopy can provide deeper

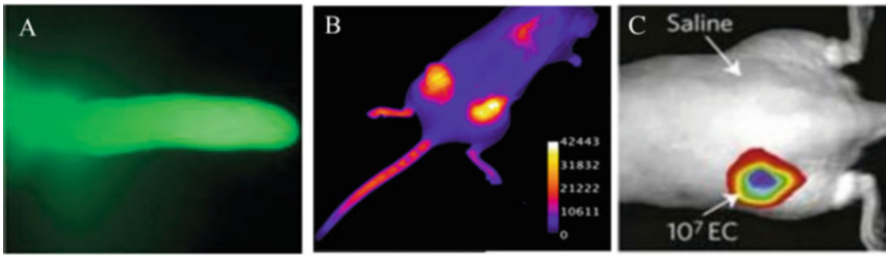

Fig. 6 Images of fluorescent imaging with organic probes. (**a**) Images of zebra fish eyes treated with fluorescent probe (Adapted from the Ref. [97] with permission); (**b**) images were acquired 48 h after injection of 200 nmol of organic fluorescent probe-chiral porphyrazine (pz), H_2[pz(trans-A_2B_2)], by tail-vein intravenous injection in mice bearing MDA-231 human breast xenograft tumors (Adapted from the Ref. [115] with permission); (**c**) fluorescence image of a rat showing that MDP-2 can image 107 *E. coli* CFUs in vivo (Adapted from the Ref. [123] with permission)

penetration depth and prolonged observation time. 6-(benzo[d]thiazol-2′-yl)-2-(N, N-dimethylamino)naphthalene (BTDAN) with disulfide group was developed as reporter and triphenylphosphonium salt as mitochondrial targeting site. This thiol reporter system provided selectivity and low cytotoxicity without the pH interference [99].

3.3 pH Imaging

pH measurement is important because various diseases such as cancer, immune dysfunction, and cystic fibrosis are associated with acid/base homeostasis [100–102]. Small molecules [103–107] and nanoparticles [108–110] have been employed for the ratiometric determination of pH. For example, a nanoplatform was designed by coupling of a pH-sensitive dye, cyanine HCyC-646, or a pH-insensitive dye, Cy 7, to the bacteriophage for the pH ratiometric imaging. The emission from bacteriophage probe conjugated with HCyC-646 varies with the change of pH, whereas the signal of probe with Cy 7 remained the same. In addition, intracellular ratiometric pH map in RAW cells was obtained by fluorescence imaging of bacteriophage probe with HCyC-646 [111]. Also, a pH-sensitive dendritic nanoprobe using pentaerythritol as the core was developed, demonstrating that nanoprobes incubated at pH 4.5 presented six times higher fluorescence than that incubated at pH 7. Fluorescent lifetime and intensity of nanoprobes for NIR fluorescent dyes could be activated in acidic environment owing to acid-sensitive linkage formed between fluorescent dye and dendritic scaffold. The fluorescence intensity and lifetime can provide both physiological and molecular information. This nanosystem with pH-sensitive linkages can be used to noninvasively detect and analyze acidic tissues with high sensitivity and specificity [112]. Another example is a NIR fluorescence

probe composed of 4′-(aminomethylphenyl)-2,2′:6′,2″-terpyridine (Tpy) and tricarbocyanine (Cy) that could detect the minor pH fluctuation in the range of 6.7–7.9 in vivo. Furthermore, real-time imaging of pH was obtained in living HepG2 and HL-7702 cells. The probe did not exhibit autofluorescence and can provide fluorescence contrast with high sensitivity, excellent photostability, and remarkable cell membrane permeability [113].

3.4 Cancer Imaging

The typical distribution of phospholipid can be disrupted when cells are at the stage of apoptosis. Therefore, targeting phosphatidylserine on the membrane surface would be useful to evaluate the treatment efficacy. Porphyrin-ytterbium complex was designed as a marker to distinguish tumor cells from normal cells because the fluorescence of porphyrin ytterbium complex can strongly bind to phosphatidylserine for tumor cell targeting [114]. Another example for cancer cell imaging is a porphyrin derivative, a chiral porphyrazine that exhibits remarkable accumulation of tumor cell in vivo, especially in breast tumor cells. It showed that the high selectivity of chiral porphyrazine for tumor cell in vivo is a critical factor in the cancer therapy [115] (see Fig. 6b). Optimized analogues of chiral porphyrazine with enhanced photophysical properties were synthesized for applications in cancer imaging [116]. BODIPY polymer with emission wavelength in NIR range conjugated with cancer-homing peptide residues could be employed for fluorescence imaging of cancer cells, and compared with original polymer, the conjugate has higher water solubility, more excellent photostability, better biocompatibility, and specific interaction to breast tumor cells [117]. Another recent study showed that 2,4,6-trisubstituted pyridine-based fluorescent probe that is pH-dependent displayed selectivity, photostability, and reversibility so that the HeLa cancer cells could be distinguished from other cells in a pH range of 2.2–7.0 [118].

3.5 Bacterial Imaging

Bacterial imaging is an emerging technology that can be used in a wide variety of fields such as food science and biomedicines. Compared to mammalian membranes, bacterial ones have some unique characterizations that can act as targets for antimicrobial drug candidate such as peptidoglycan cell wall on bacteria and yeast [119] or O-antigen unit of lipopolysaccharide on the outer membrane of gram-negative bacteria [120] or anionic phospholipids (e.g., phosphatidylglycerol) [121]. Fluorescence and radiolabeling are two contrast methods for bacterial imaging. For example, zinc dipicolylamine (Zn-DPA) complexes (probe 1) were made to selectively target the surface of bacterial cells because they have high affinity for bilayer membrane with anionic phospholipids. Bis(Zn-DPA), probe 2, was also synthesized.

Probes 1 and 2 can effectively target gram-negative and gram-positive bacteria. These compounds also preferentially stain bacteria compared to mammalian cells [122]. In addition, detection of small numbers of bacteria would be beneficial for early detection of inflammation. To achieve that, maltodextrin-based imaging probes (MDPs) were designed for bacterial infection imaging in vivo, including *E. coli*, *P. aeruginosa*, *S. aureus*, and *B. subtilis* detection [123] (see Fig. 6c). MDP could be selectively internalized to bacterial MDPs made by conjugating a fluorescent dye to maltohexaose so that the bacteria can be selectively internalized through maltodextrin transport pathway. This represents the first targeting strategy that can deliver an imaging probe as low as millimolar to bacteria. Another type of MDP could accurately image bacterial infections in rat injected with *E. coli* with excellent fluorescent intensity compared to uninfected controls.

4 Prospective and Conclusions

Fluorescence imaging has emerged as a powerful tool for diagnosis and treatment with high sensitivity, good biocompatibility, and noninvasiveness [124–126]. Conventional imaging modalities such as CT, MRI, and radionuclide imaging involve using contrast agents that are "always on" [127]. In these cases, the "always on" probes are not able to well distinguish the target tissues/cells and their proximity, leading to considerable background [128]. One unique feature of fluorescence imaging is that probes can be designed to be activatable in response to certain biological environments such as enzymatic digestion or acidification. In addition, compared to inorganic fluorescence probes, organic fluorescent probes have many advantages such as larger molar extinction coefficient in the deep NIR regions, relatively higher quantum yields, better photostability, and great biocompatibility (e.g., in zwitterionic structures and nanoformulation forms) [129, 130]. The molecular interactions such as hydrophobic and electrostatic interactions and hydrogen bonding between organic fluorescent dyes and biological species can lead to better sensitivity, selectivity, and bio-imaging capacity for diagnostics [131]. While inorganic fluorescence probes have unique properties, potential lack of body clearance and toxicity of inorganic probes may be a limiting safety concern. For example, Cd and Pb metals show high toxicity profile, and Ag- and Hg-based materials need more careful assessment [132]. On the other hand, there are also challenges and corresponding strategies for fluorescence imaging development. For example, due to the light scattering and attenuation, fluorescence might suffer from limited depth penetration, and also it is difficult to provide quantitative and tomographic information. Therefore, numerous multimodal imaging modalities were developed to complement each other. However, no imaging contrast for fused imaging has been approved by the FDA yet probably because it is still questionable whether a single probe for multimodalities is better than a mixture of two [133].

Further efforts will be made to improve imaging methods and probe development in the aspects of imaging techniques and instrument, contrast agents, and synthetic methodology. For example, multimodal imaging modalities fused with fluorescence imaging have attracted attention in order to achieve enhanced imaging depth and more accurate and comprehensive diagnosis [62, 134, 135]. Imaging-guided surgery and personalized medicine continue to be the hot research areas to solve some unmet medical needs. Meanwhile, fluorescence probes with longer wavelength are desired and advantageous for bio-imaging owing to the minimum photodamage and deeper tissue penetration [10, 136]. To conclude, in this chapter we have briefly discussed some representative fluorescent dyes including ICG, NADH/FAD, porphyrin, phthalocyanine, naphthalocyanine, BODIPY, and rhodamine, followed by some of their applications. With ongoing research efforts, fluorescence imaging using organic fluorophores has potential to make significant contributions for diagnosis and bio-imaging.

Acknowledgments We thank the Tianjin University Start-up Funding and the Chinese One-thousand Young Talent Funding.

Compliance with Ethical Standards

Funding: This chapter was made possible by Tianjin University Start-up Funding.

Conflict of Interest: The authors declare no conflict of interest.

Ethical Approval: This chapter does not contain any studies with human participants or animals performed by any of the authors.

References

1. Rao J, Dragulescu-Andrasi A, Yao H (2007) Fluorescence imaging in vivo: recent advances. Curr Opin Biotechnol 18:17–25
2. Gopalakrishnan V et al (2019) Use of CT imaging to quantify progression and response to treatment in lymphangioleiomyomatosis. Chest 155:962–971
3. Jeon SK et al (2019) Prospective evaluation of hepatic steatosis using ultrasound attenuation imaging in patients with chronic liver disease with magnetic resonance imaging proton density fat fraction as the reference standard. Ultrasound Med Biol 45:1407–1416
4. Bu L, Shen B, Cheng Z (2014) Fluorescent imaging of cancerous tissues for targeted surgery. Adv Drug Deliv Rev 76:21–38
5. Kobayashi H, Ogawa M, Alford R, Choyke PL, Urano Y (2010) New strategies for fluorescent probe design in medical diagnostic imaging. Chem Rev 110:2620–2640
6. Ponnuvel K, Kumar M, Padmini V (2016) A new quinoline-based chemosensor for Zn2+ ions and their application in living cell imaging. Sens Actuators B Chem 227:242–247
7. Callan JF, de Silva AP, Magri DC (2005) Luminescent sensors and switches in the early 21st century. Tetrahedron 61:8551–8588
8. Wang Z et al (2019) A novel isolongifolanone based fluorescent probe with super selectivity and sensitivity for hypochlorite and its application in bio-imaging. Anal Chim Acta 1051:169–178
9. Alfano RR, Demos SG, Gayen SK (1997) Advances in optical imaging of biomedical mediaa. Ann N Y Acad Sci 820:248–271

10. Yuan L, Lin W, Zheng K, He L, Huang W (2012) Far-red to near infrared analyte-responsive fluorescent probes based on organic fluorophore platforms for fluorescence imaging. Chem Soc Rev 42:622–661
11. Frangioni JV (2003) In vivo near-infrared fluorescence imaging. Curr Opin Chem Biol 7:626–634
12. Ding F, Zhan Y, Lu X, Sun Y (2018) Recent advances in near-infrared II fluorophores for multifunctional biomedical imaging. Chem Sci 9:4370–4380
13. Wang X et al (2019) LuPO4:Nd3+ nanophosphors for dual-mode deep tissue NIR-II luminescence/CT imaging. JOL 209:420–426
14. Cao Z et al (2018) Semiconducting polymer-based nanoparticles with strong absorbance in NIR-II window for in vivo photothermal therapy and photoacoustic imaging. Biomaterials 155:103–111
15. Li X et al (2019) 808 nm laser-triggered NIR-II emissive rare-earth nanoprobes for small tumor detection and blood vessel imaging. Mater Sci Eng C 100:260–268
16. Xue Z, Zeng S, Hao J (2018) Non-invasive through-skull brain vascular imaging and small tumor diagnosis based on NIR-II emissive lanthanide nanoprobes beyond 1500 nm. Biomaterials 171:153–163
17. Gonçalves MST (2008) Fluorescent labeling of biomolecules with organic probes. Chem Rev 109:190–212
18. McCorquodale EM, Colyer CL (2001) Indocyanine green as a noncovalent, pseudofluorogenic label for protein determination by capillary electrophoresis. Electrophoresis 22:2403–2408
19. Rubens FD, Ruel M, Fremes SE (2002) A new and simplified method for coronary and graft imaging during CABG. Heart Surg Forum 5:141–144
20. Mitsuhashi N et al (2008) Usefulness of intraoperative fluorescence imaging to evaluate local anatomy in hepatobiliary surgery. J Hepatobiliary Pancreat Surg 15:508–514
21. Ishizawa T et al (2009) Intraoperative fluorescent cholangiography using indocyanine green: a biliary road map for safe surgery. J Am Coll Surg 208:e1–e4
22. Ishizawa T et al (2010) Fluorescent cholangiography illuminating the biliary tree during laparoscopic cholecystectomy. Br J Surg 97:1369–1377
23. Raabe A et al (2005) Prospective evaluation of surgical microscope – integrated intraoperative near-infrared indocyanine green videoangiography during aneurysm surgery. J Neurosurg 103:982–989
24. Stummer W et al (2000) Fluorescence-guided resection of glioblastoma multiforme utilizing 5-ALA-induced porphyrins: a prospective study in 52 consecutive patients. J Neurosurg 93:1003–1013
25. Peng Q et al (1997) 5-Aminolevulinic acid-based photodynamic therapy. Cancer 79:2282–2308
26. Stummer W et al (2006) Fluorescence-guided surgery with 5-aminolevulinic acid for resection of malignant glioma: a randomised controlled multicentre phase III trial. Lancet Oncol 7:392–401
27. Schucht P et al (2012) Gross total resection rates in contemporary glioblastoma surgery: results of an institutional protocol combining 5-aminolevulinic acid intraoperative fluorescence imaging and brain mapping. Neurosurgery 71:927–936
28. Puppa AD et al (2013) 5-aminolevulinic acid (5-ALA) fluorescence guided surgery of high-grade gliomas in eloquent areas assisted by functional mapping. Our experience and review of the literature. Acta Neurochir 155:965–972
29. Tummers QRJG et al (2014) Real-time intraoperative detection of breast cancer using near-infrared fluorescence imaging and methylene blue. Eur J Surg Oncol 40:850–858
30. van der Vorst JR et al (2014) Intraoperative near-infrared fluorescence imaging of parathyroid adenomas with use of low-dose methylene blue. Head neck-J. Sci. Spec. Head Neck 36:853–858
31. Kolemen S, Akkaya EU (2018) Reaction-based BODIPY probes for selective bio-imaging. Coord Chem Rev 354:121–134

32. Rurack K, Kollmannsberger M, Daub J (2001) A highly efficient sensor molecule emitting in the near infrared (NIR): 3,5-distyryl-8-(p-dimethylaminophenyl)difluoroboradiaza-s-indacene. New J Chem 25:289–292
33. Saki N, Dinc T, Akkaya EU (2006) Excimer emission and energy transfer in cofacial boradiazaindacene (BODIPY) dimers built on a xanthene scaffold. Tetrahedron 62:2721–2725
34. Goud TV, Tutar A, Biellmann J-F (2006) Synthesis of 8-heteroatom-substituted 4,4-difluoro-4-bora-3a,4a-diaza-s-indacene dyes (BODIPY). Tetrahedron 62:5084–5091
35. Benniston AC, Copley G (2009) Lighting the way ahead with boron dipyrromethene (Bodipy) dyes. Phys Chem Chem Phys 11:4124–4131
36. Loudet A, Burgess K (2007) BODIPY dyes and their derivatives: syntheses and spectroscopic properties. Chem Rev 107:4891–4932
37. Ulrich G, Ziessel R, Harriman A (2008) The chemistry of fluorescent bodipy dyes: versatility unsurpassed. Angew Chem Int Ed 47:1184–1201
38. Ma X, Tan Z, Wei G, Wei D, Du Y (2012) Solvent controlled sugar-rhodamine fluorescence sensor for Cu(2+) detection. Analyst 137:1436–1439
39. Senthil Murugan A, Vidhyalakshmi N, Ramesh U, Annaraj J (2018) In vivo bio-imaging studies of highly selective, sensitive rhodamine based fluorescent chemosensor for the detection of Cu2+/Fe3+ ions. Sens Actuators B Chem. 274:22–29
40. Shen S-L, Zhang X-F, Ge Y-Q, Zhu Y, Cao X-Q (2018) A novel ratiometric fluorescent probe for the detection of HOCl based on FRET strategy. Sens Actuators B Chem 254:736–741
41. Kilic H, Bozkurt E (2018) A rhodamine-based novel turn on trivalent ions sensor. J Photochem Photobiol A Chem 363:23–30
42. Palero JA, De Bruijn HS, Sterenborg H, Gerritsen HC (2006) In vivo nonlinear spectral imaging in mouse skin. Opt Express 14:4395–4402
43. Skala MC et al (2007) In vivo multiphoton microscopy of NADH and FAD redox states, fluorescence lifetimes, and cellular morphology in precancerous epithelia. Proc Natl Acad Sci U S A 104:19494–19499
44. Schweitzer D et al (2007) Towards metabolic mapping of the human retina. Microsc Res Tech 70:410–419
45. Yu Q, Heikal AA (2009) Two-photon autofluorescence dynamics imaging reveals sensitivity of intracellular NADH concentration and conformation to cell physiology at the single-cell level. J Photochem Photobiol B Biol 95:46–57
46. Ghukasyan VV, Kao F-J (2009) Monitoring cellular metabolism with fluorescence lifetime of reduced Nicotinamide adenine dinucleotide. J Phys Chem C 113:11532–11540
47. Huang S, Heikal AA, Webb WW (2002) Two-photon fluorescence spectroscopy and microscopy of NAD(P)H and flavoprotein. Biophys J 82:2811–2825
48. Yaseen MA et al (2013) In vivo imaging of cerebral energy metabolism with two-photon fluorescence lifetime microscopy of NADH. Biomed Opt Express 4:307–321
49. Wang H-P et al (2007) Fluorescence lifetime image of a single halobacterium. Chem Phys Lett 442:441–444
50. Nakabayashi T, Wang H-P, Kinjo M, Ohta N (2008) Application of fluorescence lifetime imaging of enhanced green fluorescent protein to intracellular pH measurements. Photochem Photobiol Sci 7:668–670
51. Ogikubo S et al (2011) Intracellular pH sensing using autofluorescence lifetime microscopy. J Phys Chem B 115:10385–10390
52. Nakabayashi T et al (2008) Stress-induced environmental changes in a single cell as revealed by fluorescence lifetime imaging. Photochem Photobiol Sci 7:671–674
53. Ito T et al (2009) Fluorescence lifetime images of green fluorescent protein in HeLa cells during TNF-α induced apoptosis. Photochem Photobiol Sci 8:763–767
54. Awasthi K, Nakabayashi T, Ohta N (2012) Application of nanosecond pulsed electric fields into HeLa cells expressing enhanced green fluorescent protein and fluorescence lifetime microscopy. J Phys Chem B 116:11159–11165

55. Wallrabe H, Periasamy A (2005) Imaging protein molecules using FRET and FLIM microscopy. Curr Opin Biotechnol 16:19–27
56. Ackroyd R, Kelty C, Brown N, Reed M (2001) The history of photodetection and photodynamic therapy. Photochem Photobiol 74:656–669
57. Auler H, Banzer G (1942) Untersuchungen über die Rolle der Porphyrine bei geschwulstkranken Menschen und Tieren. Z Krebsforsch 53:65–68
58. Josefsen LB, Boyle RW (2008) Photodynamic therapy and the development of metal-based photosensitisers. Met Based Drugs 2008:276109
59. Wilson BC, Patterson MS (2008) The physics, biophysics and technology of photodynamic therapy. Phys Med Biol 53:R61–R109
60. Blake E, Allen J, Curnow A (2011) An in vitro comparison of the effects of the iron-chelating agents, CP94 and dexrazoxane, on protoporphyrin IX accumulation for photodynamic therapy and/or fluorescence guided resection. Photochem Photobiol 87:1419–1426
61. Winkelman J (1962) The distribution of tetraphenylporphinesulfonate in the tumor-bearing rat. Cancer Res 22:589–596
62. Lovell JF et al (2011) Porphysome nanovesicles generated by porphyrin bilayers for use as multimodal biophotonic contrast agents. Nat Mater 10:324–332
63. Huang H et al (2017) Implantable tin porphyrin-PEG hydrogels with pH-responsive fluorescence. Biomacromolecules 18:562–567
64. Huang H et al (2014) Pd-porphyrin-cross-linked implantable hydrogels with oxygen-responsive phosphorescence. Adv Healthc Mater 3:891–896
65. Wong RCH, Lo P-C, Ng DKP (2019) Stimuli responsive phthalocyanine-based fluorescent probes and photosensitizers. Coord Chem Rev 379:30–46
66. van Leengoed HL et al (1994) In vivo fluorescence and photodynamic activity of zinc phthalocyanine administered in liposomes. Br J Cancer 69:840–845
67. Taratula O et al (2015) Naphthalocyanine-based biodegradable polymeric nanoparticles for image-guided combinatorial phototherapy. Chem Mater 27:6155–6165
68. Gasser M, Waaga-Gasser AM (2016) Therapeutic antibodies in cancer therapy. Adv Exp Med Biol 917:95–120
69. Fay F, Scott CJ (2011) Antibody-targeted nanoparticles for cancer therapy. Immunotherapy 3:381–394
70. Alibakhshi A et al (2017) Targeted cancer therapy through antibody fragments-decorated nanomedicines. J Control Release 268:323–334
71. Hollandsworth HM et al (2019) Anti-Claudin-1 conjugated to a near-infrared Fluorophore targets colon cancer in PDOX mouse models. J Surg Res 242:145–150
72. Maawy AA et al (2015) Near infra-red photoimmunotherapy with anti-CEA-IR700 results in extensive tumor lysis and a significant decrease in tumor burden in orthotopic mouse models of pancreatic cancer. PLoS One 10:e0121989
73. Hiroshima Y et al (2015) Photoimmunotherapy inhibits tumor recurrence after surgical resection on a pancreatic cancer patient-derived orthotopic xenograft (PDOX) nude mouse model. Ann Surg Oncol 22(Suppl 3):S1469–S1474
74. Boogerd LSF et al (2018) Safety and effectiveness of SGM-101, a fluorescent antibody targeting carcinoembryonic antigen, for intraoperative detection of colorectal cancer: a dose-escalation pilot study. Lancet Gastroenterol Hepatol 3:181–191
75. Kijanka M et al (2013) Rapid optical imaging of human breast tumour xenografts using anti-HER2 VHHs site-directly conjugated to IRDye 800CW for image-guided surgery. Eur J Nucl Med Mol Imaging 40:1718–1729
76. van der Vorst JR et al (2013) Near-infrared fluorescence-guided resection of colorectal liver metastases. Cancer 119:3411–3418
77. van der Vorst JR et al (2011) Optimization of near-infrared fluorescent sentinel lymph node mapping in cervical cancer patients. Int J Gynecol Cancer 21:1472–1478
78. Crane LMA et al (2011) Intraoperative multispectral fluorescence imaging for the detection of the sentinel lymph node in cervical cancer: a novel concept. Mol Imaging Biol 13:1043–1049

79. Fujiwara M, Mizukami T, Suzuki A, Fukamizu H (2009) Sentinel lymph node detection in skin cancer patients using real-time fluorescence navigation with indocyanine green: preliminary experience. J Plast Reconstr Aesthet Surg 62:E373–E378
80. van der Vorst JR et al (2013) Dose optimization for near-infrared fluorescence sentinel lymph node mapping in patients with melanoma. Br J Dermatol 168:93–98
81. van Dam GM et al (2011) Intraoperative tumor-specific fluorescence imaging in ovarian cancer by folate receptor-alpha targeting: first in-human results. Nat Med 17:1315–U202
82. Tsujino Y, Mizumoto K, Matsuzaka Y, Niihara H, Morita E (2009) Fluorescence navigation with indocyanine green for detecting sentinel nodes in extramammary Paget's disease and squamous cell carcinoma. J Dermatol 36:90–94
83. Yokoyama N et al (2012) Real-time detection of hepatic micrometastases from pancreatic cancer by intraoperative fluorescence imaging preliminary results of a prospective study. Cancer 118:2813–2819
84. Suzuki T et al (2013) Cadherin 13 overexpression as an important factor related to the absence of tumor fluorescence in 5-aminolevulinic acid-guided resection of glioma laboratory investigation. J Neurosurg 119:1331–1339
85. Loja MN et al (2013) Optical molecular imaging detects changes in extracellular pH with the development of head and neck cancer. Int J Cancer 132:1613–1623
86. Sevick-Muraca EM (2012) Translation of near-infrared fluorescence imaging technologies: emerging clinical applications. Annu Rev Med 63:217–231
87. Wapnir I et al (2014) Intraoperative imaging of nipple perfusion patterns and ischemic complications in nipple-sparing mastectomies. Ann Surg Oncol 21:100–106
88. Vahrmeijer AL, Hutteman M, van der Vorst JR, van de Velde CJH, Frangioni JV (2013) Image-guided cancer surgery using near-infrared fluorescence. Nat Rev Clin Oncol 10:507–518
89. van der Vorst JR et al (2012) 46. Near-infrared fluorescence sentinel lymph node mapping of the oral cavity in head and neck cancer patients. Eur J Surg Oncol 38:745
90. Chi C et al (2014) Intraoperative imaging-guided Cancer surgery: from current fluorescence molecular imaging methods to future multi-modality imaging technology. Theranostics 4:1072–1084
91. Nguyen QT, Tsien RY (2013) Fluorescence-guided surgery with live molecular navigation – a new cutting edge. Nat Rev Cancer 13:653–662
92. He L, Yang X, Xu K, Kong X, Lin W (2017) A multi-signal fluorescent probe for simultaneously distinguishing and sequentially sensing cysteine/homocysteine, glutathione, and hydrogen sulfide in living cells. Chem Sci 8:6257–6265
93. Zhang L et al (2016) A highly selective and sensitive near-infrared fluorescent probe for imaging of hydrogen sulphide in living cells and mice. Sci Rep 6:18868
94. Xie X, Yin C, Yue Y, Chao J, Huo F (2018) Fluorescent probe detect distinguishly sulfite/hydrogen sulfide and thiol via two emission channels in vivo. Sens Actuators B Chem 277:647–653
95. Yin J et al (2016) Correction to 'cyanine-based fluorescent probe for highly selective detection of glutathione in cell cultures and live mouse tissues'. J Am Chem Soc 138:7442
96. Zhang X et al (2019) Mitochondria-targeting near-infrared ratiometric fluorescent probe for selective imaging of cysteine in orthotopic lung cancer mice. Sens Actuators B Chem 282:69–77
97. Chen X, Ko S-K, Kim MJ, Shin I, Yoon J (2010) A thiol-specific fluorescent probe and its application for bioimaging. Chem Commun 46:2751–2753
98. Zhu B et al (2010) A colorimetric and ratiometric fluorescent probe for thiols and its bioimaging applications. Chem Commun 46:5710–5712
99. Lim CS et al (2011) Ratiometric detection of mitochondrial thiols with a two-photon fluorescent probe. J Am Chem Soc 133:11132–11135
100. Kellum JA, Song M, Li J (2004) Science review: extracellular acidosis and the immune response: clinical and physiologic implications. Crit Care 8:331

101. Coakley RD et al (2003) Abnormal surface liquid pH regulation by cultured cystic fibrosis bronchial epithelium. Proc Natl Acad Sci 100:16083–16088
102. Gillies RJ, Schomack PA, Secomb TW, Raghunand N (1999) Causes and effects of heterogeneous perfusion in tumors. Neoplasia 1:197–207
103. Overly CC, Lee K-D, Berthiaume E, Hollenbeck PJ (1995) Quantitative measurement of intraorganelle pH in the endosomal-lysosomal pathway in neurons by using ratiometric imaging with pyranine. Proc Natl Acad Sci 92:3156–3160
104. Martin GR, Jain RK (1993) Fluorescence ratio imaging measurement of pH gradients: calibration and application in normal and tumor tissues. Microvasc Res 46:216–230
105. Bassnett S, Reinisch L, Beebe DC (1990) Intracellular pH measurement using single excitation-dual emission fluorescence ratios. Am J Physiol 258:C171–C178
106. Murphy RF, Powers S, Cantor CR (1984) Endosome pH measured in single cells by dual fluorescence flow cytometry: rapid acidification of insulin to pH 6. J Cell Biol 98:1757–1762
107. Thomas JA, Buchsbaum RN, Zimniak A, Racker E (1979) Intracellular pH measurements in Ehrlich ascites tumor cells utilizing spectroscopic probes generated in situ. Biochemistry 18:2210–2218
108. Kim S, Pudavar HE, Prasad PN (2006) Dye-concentrated organically modified silica nanoparticles as a ratiometric fluorescent pH probe by one-and two-photon excitation. Chem Commun 19:2071–2073
109. McNamara KP et al (2001) Synthesis, characterization, and application of fluorescence sensing lipobeads for intracellular pH measurements. Anal Chem 73:3240–3246
110. Ji J, Rosenzweig N, Griffin C, Rosenzweig Z (2000) Synthesis and application of submicrometer fluorescence sensing particles for lysosomal pH measurements in murine macrophages. Anal Chem 72:3497–3503
111. Marshall MV et al (2010) Near-infrared fluorescence imaging in humans with indocyanine green: a review and update. Open Surg Oncol J 2:12–25
112. Almutairi A, Guillaudeu SJ, Berezin MY, Achilefu S, Fréchet JMJ (2008) Biodegradable pH-sensing dendritic Nanoprobes for near-infrared fluorescence lifetime and intensity imaging. J Am Chem Soc 130:444–445
113. Tang B et al (2009) A near-infrared neutral pH fluorescent probe for monitoring minor pH changes: imaging in living HepG2 and HL-7702 cells. J Am Chem Soc 131:3016–3023
114. Zhang T et al (2013) Porphyrin-based ytterbium complexes targeting anionic phospholipid membranes as selective biomarkers for cancer cell imaging. Chem Commun 49:7252–7254
115. Trivedi ER et al (2010) Chiral porphyrazine near-IR optical imaging agent exhibiting preferential tumor accumulation. Proc Natl Acad Sci 107:1284–1288
116. Trivedi ER et al (2010) Synthesis of heteroatom substituted naphthoporphyrazine derivatives with near-infrared absorption and emission. J Org Chem 75:1799–1802
117. Zhu S et al (2013) Highly water-soluble, near-infrared emissive BODIPY polymeric dye bearing RGD peptide residues for cancer imaging. Anal Chim Acta 758:138–144
118. Ma J et al (2018) A small molecular pH-dependent fluorescent probe for cancer cell imaging in living cell. Talanta 182:464–469
119. Cooper MA, Williams DH (1999) Binding of glycopeptide antibiotics to a model of a vancomycin-resistant bacterium. Chem Biol 6:891–899
120. Kotra LP, Amro NA, Liu GY, Mobashery S (2000) Visualizing bacteria at high resolution. ASM News 66:675–681
121. Fernandez-Lopez S et al (2001) Antibacterial agents based on the cyclic D,L-alpha-peptide architecture. Nature 412:452–455
122. Leevy WM et al (2006) Optical imaging of bacterial infection in living mice using a fluorescent near-infrared molecular probe. J Am Chem Soc 128:16476–16477
123. Ning X et al (2011) Maltodextrin-based imaging probes detect bacteria in vivo with high sensitivity and specificity. Nat Mater 10:602–607

124. Wang L, Xia Q, Liu R, Qu J (2018) A red fluorescent probe for ribonucleic acid (RNA) detection, cancer cell tracing and tumor growth monitoring. Sens Actuators B Chem 273:935–943
125. Cal PMSD et al (2016) Site-selective installation of BASHY fluorescent dyes to Annexin V for targeted detection of apoptotic cells. Chem Commun 53:368–371
126. Georgiev NI, Krasteva PV, Bojinov VB (2019) A ratiometric 4-amido-1,8-naphthalimide fluorescent probe based on excimer-monomer emission for determination of pH and water content in organic solvents. JOL 212:271–278
127. Weissleder R, Pittet MJ (2008) Imaging in the era of molecular oncology. Nature 452:580–589
128. Kobayashi H, Choyke PL (2011) Target-cancer-cell-specific activatable fluorescence imaging probes: rational design and in vivo applications. Acc Chem Res 44:83–90
129. Wang L, Zhuo S, Tang H, Cao D (2018) A near-infrared turn on fluorescent probe for cysteine based on organic nanoparticles. Sens Actuators B Chem 277:437–444
130. Martinić I, Eliseeva SV, Petoud S (2017) Near-infrared emitting probes for biological imaging: organic fluorophores, quantum dots, fluorescent proteins, lanthanide(III) complexes and nanomaterials. JOL 189:19–43
131. Kim D, Ryu HG, Ahn KH (2014) Recent development of two-photon fluorescent probes for bioimaging. Org Biomol Chem 12:4550–4566
132. Chinnathambi S, Shirahata N (2019) Recent advances on fluorescent biomarkers of near-infrared quantum dots for in vitro and in vivo imaging. Sci Technol Adv Mater 20:337–355
133. Zhao J et al (2018) Recent developments in multimodality fluorescence imaging probes. Acta Pharm Sin B 8:320–338
134. Rieffel J et al (2015) Hexamodal imaging with porphyrin-phospholipid-coated upconversion nanoparticles. Adv Mater 27:1785–1790
135. Zhang Y et al (2016) Surfactant-stripped frozen pheophytin micelles for multimodal gut imaging. Adv Mater 28:8524–8530
136. Zhou Y et al (2016) A phosphorus phthalocyanine formulation with intense absorbance at 1000 nm for deep optical imaging. Theranostics 6:688–697